

# Fast spin-valley-based quantum gates in Si with micromagnets

Peihao Huang<sup>1\*</sup> and Xuedong Hu<sup>2</sup>

<sup>1</sup>*Shenzhen Institute for Quantum Science and Engineering, and Department of Physics, Southern University of Science and Technology, Shenzhen 518055, China*

<sup>2</sup>*Department of Physics, University at Buffalo, SUNY, Buffalo, New York 14260*

(Dated: June 7, 2022)

Micromagnets have been employed recently to achieve high-fidelity spin manipulation and strong spin-photon coupling, which paves the way for the future scale-up of spin qubits in silicon quantum dots. However, experiments on spin relaxation in silicon with micromagnets show a magnetic field dependence clearly different from previous theoretical and experimental results without micromagnets. We reveal that a synthetic spin-orbit field from micromagnets leads to such signatures in spin relaxation, where the interference effect plays a critical role. Furthermore, we show an enhancement of the electric dipole spin resonance and spin-photon coupling in a synthetic spin-orbit field as a result of the interference effect and the strong mixing at the spin-valley hotspot. The results enable novel schemes for fast quantum gates with potential applications in semiconducting quantum computing.

Silicon quantum dot (QD) presents an attractive platform for spin qubits, with long spin coherence times, strong exchange interaction, and fabrication technologies backed by the massive microelectronics industry [1–11]. Meanwhile, the employment of micromagnets and their associated synthetic spin-orbit coupling (s-SOC) allows fast electric dipole spin resonance (EDSR) [12–27]. Recent experimental demonstrations of high-fidelity single- and two-qubit gates [9, 10, 17] have clearly confirmed spin qubits in silicon as a promising building block for a future scalable quantum computer.

Significant challenges remain toward a scalable Si-based quantum computer. Micromagnets open new spin decoherence channels via environmental electrical noise [17, 25, 27]. The experiments of spin relaxation with micromagnets show different magnetic field dependence from the experiments without micromagnets [22, 24]. On the other hand, the valley states from the conduction band degeneracy of silicon [28] could introduce unwanted dynamics and leakage. A particularly intriguing parameter regime is near the spin-valley hotspot (SVH) [22, 25, 26, 29–33], where electron Zeeman splitting and valley splitting are near resonance, spin relaxation is greatly enhanced because of the spin-valley mixing (SVM). A careful examination of SVM in the presence of a micromagnet, from the perspectives of both spin relaxation and manipulation, remains an open problem.

In this Letter, we first reveal that the experimental signatures of spin relaxation, at both the high and low magnetic field, are perfectly captured by our theory, in which broken time-reversal symmetry ( $\mathcal{T}$ -symmetry) of s-SOC leads to constructive interference between the SVM paths. We then show a significant enhancement of EDSR and spin-photon coupling via the s-SOC as a result of the constructive interference and the strong mixing near the SVH. Accounting for both the faster decoherence and manipulation, we find the quality factors for the EDSR and the spin-photon coupling peak near the hotspot, such

that the relaxation hotspot is beneficial for rapid high-fidelity quantum gates. Our work may stimulate explorations of the benefits of the valley degree of freedom and the effects of symmetry and interference on solid-state qubits.

*Model Hamiltonian*— We consider an electron spin qubit in a gated-defined silicon QD in the presence of a micromagnet and an applied magnetic field (Fig. 1 a). The model Hamiltonian is  $H = H_S + H_O + H_{SO} + V_{ext}(\vec{r}, t)$ , where  $H_S$  is the bare Hamiltonian of the spin qubit,  $H_O = H_V + H_D$  is the orbital Hamiltonian consists of the valley term  $H_V$  and the intra-valley orbital term  $H_D$ ,  $H_{SO}$  is the SOC Hamiltonian, and  $V_{ext}$  is the electric potential from noise or a manipulation field [30]. The total magnetic field  $\vec{B}(\vec{r}) = \vec{B}_0 + \vec{B}_1(\vec{r})$  consists of a uniform  $\vec{B}_0$  and a position-dependent  $\vec{B}_1(\vec{r})$  contribution. The former leads to the bare spin Hamiltonian  $H_S$ ,  $H_S = \frac{1}{2}E_Z\vec{\sigma} \cdot \hat{n}$ , where  $E_Z = g\mu_B B_0$  is the bare Zeeman splitting,  $\vec{\sigma}$  is the electron spin operator, and  $\hat{n}$  is the unit vector along  $\vec{B}_0$  assumed to be in-plane. The latter results in a s-SOC,  $H_{SO} = \frac{1}{2}g\mu_B\vec{\sigma} \cdot \vec{B}_1(\vec{r})$ . Without loss of generality, we assume the magnetic field gradient to be in the  $x$ -direction, such that  $H_{SO} = \frac{1}{2}g\mu_B\vec{\sigma} \cdot \vec{b}_1x$ , where  $\vec{b}_1 \equiv \partial\vec{B}_1/\partial x = [b_{1l}, 0, b_{1t}]$ . The s-SOC provides an electric knob to control a spin qubit [12], while also exposes the qubit to electrical noises. Here we study the interplay between s-SOC and valley-orbit coupling in a silicon QD, and consequences in terms of spin relaxation, manipulation, spin-photon coupling, and spin pure dephasing.

*Effective dipole and breaking of  $\mathcal{T}$ -symmetry*— An important feature of a Si QD is the presence of a low-lying valley excited state. In the presence of the s-SOC, the spin and valley states would mix, making it possible for electrically induced spin flip transitions. We denote the spin eigenstates  $|\downarrow\rangle$  and  $|\uparrow\rangle$ , and the two lowest valley eigenstates  $|v_0\rangle$  and  $|v_1\rangle$  with eigenvalues  $\pm E_{VS}/2$ , where  $E_{VS}$  is the valley splitting. The s-SOC couples  $|v_0 \uparrow\rangle$  with  $|v_1 \downarrow\rangle$  [29, 30, 34], and  $|v_0 \downarrow\rangle$  with  $|v_1 \uparrow\rangle$ , with

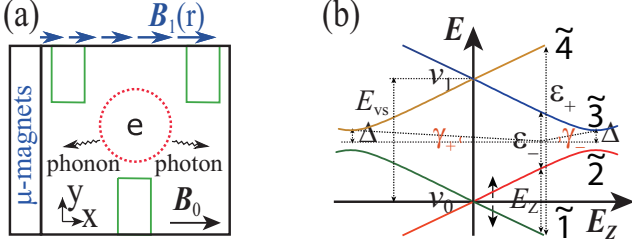


FIG. 1. Schematics plots. (a) Schematic plot of an electron spin qubit in a gate-defined QD with micro-magnets. (b) The energy level diagram of the mixed spin-valley eigenstates as a function of the Zeeman splitting. The angles  $\gamma_{\pm}$  are indicated for the different SVM.

the coupling matrix elements  $\Delta_{v_0\uparrow, v_1\downarrow} \equiv \langle v_0 \uparrow | H_{SOC} | v_1 \downarrow \rangle$  and  $\Delta_{v_0\downarrow, v_1\uparrow} \equiv \langle v_0 \downarrow | H_{SOC} | v_1 \uparrow \rangle$ . By exact diagonalization of the coupled Hamiltonian, the spin-valley eigenstates  $|\tilde{1}\rangle$ ,  $|\tilde{2}\rangle$ ,  $|\tilde{3}\rangle$ , and  $|\tilde{4}\rangle$  are obtained, with the energy spectrum shown in Fig. 1b.

With the transition dipole  $\vec{r}_i^{v_0 v_1} = \langle v_0 | \vec{r} | v_1 \rangle$  between the two eigenvalleys generally non-vanishing [29, 35], electric field can induce transitions between the spin-valley eigenstates. The relevant transition dipole for the spin-flip is  $\langle \tilde{1} | \vec{r}_i | \tilde{2} \rangle$  when  $E_Z < E_{VS}$ , and  $\langle \tilde{1} | \vec{r}_i | \tilde{3} \rangle$  when  $E_Z > E_{VS}$  [30]. The transition dipole takes the form (see Supplemental material)

$$\langle \tilde{1} | \vec{r}_i | \tilde{2} \rangle = -|\vec{r}_i^{v_0 v_1}| \sin \frac{\gamma_- + \gamma_+}{2}. \quad (1)$$

Here the angles  $\gamma_{\mp} = \tan^{-1}(\Delta/\varepsilon_{\mp})$  capture the mixing of  $|v_0 \uparrow\rangle$  with  $|v_1 \downarrow\rangle$  and  $|v_0 \downarrow\rangle$  with  $|v_1 \uparrow\rangle$ , with  $\Delta = |\Delta_{v_0\uparrow, v_1\downarrow}| = |\Delta_{v_0\downarrow, v_1\uparrow}| = |g\mu_B b_{1t} x^{v_0 v_1}/2|$  the amplitude of the spin-valley coupling matrix element, and  $\varepsilon_{\mp} = E_{VS} \mp E_Z$  the energy detunings as shown in Fig. 1b. Similarly, we have  $\langle \tilde{1} | \vec{r}_i | \tilde{3} \rangle = -|\vec{r}_i^{v_0 v_1}| \cos \frac{\gamma_- + \gamma_+}{2}$ . We emphasize that the "+" sign between  $\gamma_-$  and  $\gamma_+$  in the dipole moments arises from a constructive interference between the two SVM paths, as discussed below. In comparison, for the case of the intrinsic SOC (i-SOC) presents in the host material, the "+" sign is replaced by a "-" sign, corresponding to a destructive interference between those mixing paths.

In the limit  $\Delta \ll \varepsilon_+ \equiv E_{VS} + E_Z$ , i.e. weak spin-valley coupling as compared with valley-orbit coupling and/or Zeeman splitting, which is usually satisfied in Si QDs, the transition dipole of the spin qubit for any value of  $E_Z$  can be written as  $r_s = -|\vec{r}_i^{v_0 v_1}| \eta_{SV}$ , where

$$\eta_{SV} \approx \text{sgn}(\varepsilon_-) \sqrt{\frac{1 - C_s}{2}} + \frac{\Delta}{2\varepsilon_+} \sqrt{\frac{1 + C_s}{2}}, \quad (2)$$

with  $C_s = \left[1 + \frac{\Delta^2}{\varepsilon_-^2}\right]^{-1/2}$ . The "+" sign in front of the second term in  $\eta_{SV}$  is again from a constructive interference between the two SVM paths. Note the result of

$1/T_1$	DP	PE	JN	$1/f$	general case
i-SOC ( $E_Z < E_{VS}$ )	$B_0^7$	$B_0^5$	$B_0^3$	$B_0$	$\propto \omega_Z^2 S(\omega_Z)$
i-SOC ( $E_Z > E_{VS}$ )	$B_0^3$	$B_0$	$B_0^{-1}$	$B_0^{-3}$	$\propto \omega_Z^{-2} S(\omega_Z)$
s-SOC ( $E_Z < E_{VS}$ )	$B_0^5$	$B_0^3$	$B_0$	$B_0^{-1}$	$\propto S(\omega_Z)$
s-SOC ( $E_Z > E_{VS}$ )	$B_0$	$B_0^{-1}$	$B_0^{-3}$	$B_0^{-5}$	$\propto \omega_Z^{-4} S(\omega_Z)$

TABLE I. Spin relaxation rate  $1/T_1$  versus the magnetic field  $B_0$  due to DP phonon, PE phonon, Johnson noise (JN), or  $1/f$  charge noise via the i-SOC or the s-SOC (zero temperature is assumed).  $S(\omega_Z)$  is the power spectral density of electric field,  $\omega_Z = g\mu B_0/\hbar$  is the Larmor frequency.

$\eta_{SV}$  is valid both at and away the relaxation hotspot. When  $\Delta \approx |\varepsilon_-|$ , we can recover the previous results [29, 30]. When  $\Delta \ll |\varepsilon_-|$ ,  $\eta_{SV} = \frac{E_{VS}\Delta}{E_{VS}^2 - E_Z^2}$  (for i-SOC,  $\eta_{SV, iSOC} = \frac{E_Z\Delta}{E_{VS}^2 - E_Z^2}$ ) can be obtained perturbatively.

The sign difference in the results for s-SOC and i-SOC is due to the different relative phase between the matrix elements  $\Delta_{v_0\uparrow, v_1\downarrow}$  and  $\Delta_{v_0\downarrow, v_1\uparrow}^*$  (see Supplemental material), which are in turn determined by the property of the SOC under time-reversal operation  $\Theta$ . In particular, s-SOC breaks the  $\mathcal{T}$ -symmetry,  $\Theta H_{s-SOC} \Theta^{-1} = -H_{s-SOC}$ , so that  $\Delta_{v_0\uparrow, v_1\downarrow} = \langle \Theta(v_1 \downarrow) | \Theta H_{SOC} \Theta^{-1} | \Theta(v_0 \uparrow) \rangle = \Delta_{v_0\downarrow, v_1\uparrow}^*$ . On the other hand, i-SOC conserves the  $\mathcal{T}$ -symmetry, so that  $\Delta_{v_0\uparrow, v_1\downarrow} = -\Delta_{v_0\downarrow, v_1\uparrow}^*$ . In short, the breaking of  $\mathcal{T}$ -symmetry by s-SOC modifies the relative phase of the matrix elements  $\Delta_{v_0\uparrow, v_1\downarrow}$  (for mixing between  $|\tilde{2}\rangle$  and  $|\tilde{3}\rangle$ ) and  $\Delta_{v_0\downarrow, v_1\uparrow}^*$  (for mixing between  $|\tilde{1}\rangle$  and  $|\tilde{4}\rangle$ ), thus substantially modifies the properties of the spin qubit due to the interference between the two mixing paths.

*Spin relaxation*— The SVM due to s-SOC means that electrical noises can cause spin decoherence. In particular, the resulting spin relaxation is

$$1/T_1 = \frac{4\pi e^2}{\hbar^2} \eta_{SV}^2 (\hbar\omega_Z) \sum_i |r_i^{v_0 v_1}|^2 S_{ii}^E(\omega_Z), \quad (3)$$

where  $S_{ii}^E(\omega) \equiv \frac{1}{2\pi} \int_{-\infty}^{+\infty} d\tau \overline{E_i(0)E_i(\tau)} \cos(\omega\tau)$  is the noise spectral density ( $i = x, y, z$ ). When  $E_Z > E_{VS}$ , an additional spin relaxation channel via the intermediate state  $|\tilde{2}\rangle$  arises [29, 30]. However, its contribution to overall spin relaxation is relatively weak (see Supplemental material) and is not included here.

An important feature of spin relaxation rate  $1/T_1$  is its dependence on the magnetic field  $B_0$ . This  $B_0$ -dependence is determined by the spectral density  $S_{ii}^E(\omega_Z)$  of the electrical noise and the factor  $\eta_{SV}(\hbar\omega_Z)$  that captures the effect of the SVM. Table I summarizes the  $B_0$  dependence of  $1/T_1$  via the SVM due to deformation potential (DP) phonon, piezoelectric (PE) phonon, Johnson noise, or  $1/f$  charge noise at the zero temperature limit. At finite temperatures, an extra term  $\coth(E_Z/k_B T)$  in spectral density of Johnson and phonon noise will play a role. In particular, at the high-temperature limit when

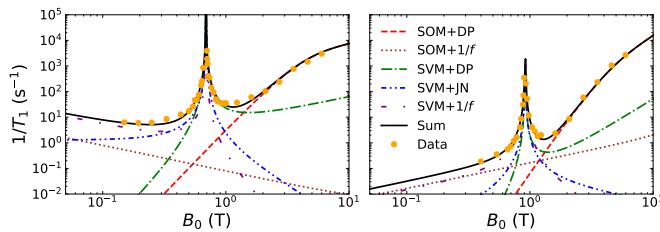


FIG. 2. Spin relaxation  $1/T_1$  in a silicon QD as a function of the magnetic field  $B_0$  due to DP phonon, Johnson noise (JN),  $1/f$  charge noise via the SVM or the intra-valley SOM. Panel (a),(b):  $1/T_1$  mediated by the s-SOC (a) or the i-SOC (b). Due to the breaking  $\mathcal{T}$ -symmetry of the s-SOC,  $1/T_1$  shows weaker dependence with  $B_0$  than the case of the i-SOC.

$T > g\mu_B B_0/k_B$ ,  $\coth(E_Z/k_B T) \approx k_B T/(g\mu_B B_0)$ , which results in extra  $1/B_0$  dependence for spin relaxation [30].

In addition to spin relaxation due to the SVM, it could also arise due to intra-valley spin-orbit mixing (SOM), which can be obtained from the result of the SVM by replacing  $E_{VS}$  and  $r_i^{v_0 v_1}$  by  $E_d$  and  $r_d = r_{d0} F_c(\omega_Z)$ , where  $E_d$  is the intra-valley orbital splitting,  $r_{d0} = \hbar/\sqrt{mE_d}$  is the transition dipole between the lowest two orbitals, and  $F_c(B_0) = e^{-\omega_Z^2 r_{d0}^2/(2v_j^2)}$  is due to the contribution beyond the electric dipole approximation and leads to phonon bottleneck effect at higher magnetic fields [36–38].

Fig. 2 shows the spin relaxation via s-SOC (left panel) or i-SOC (right panel) for devices with or without a micro-magnet. The dots are the experimental data from Ref. [22]. The lines are theoretical results for DP phonon, Johnson noise, and  $1/f$  charge noise via the SVM or the intra-valley SOM (parameters listed in the Supplemental material). Our theory faithfully captures the main features observed in the experiment. In the case with micro-magnet, the low-field spin relaxation is saturated, and is dominated by the  $1/f$  charge noise via the s-SOC induced SVM. Importantly, the broken  $\mathcal{T}$ -symmetry of the s-SOC leads to this weak  $B_0$  dependence. As  $B_0$  increases, spin relaxation is dominated by the SVM and Johnson noise, and shows  $B_0 \coth(\gamma_e B_0/k_B T_e) \sim k_B T_e/\gamma_e$  dependence that is independence with  $B_0$  at the low field limit ( $B_0 \ll k_B T_e/(g\mu_B)$ ). In comparison, spin relaxation would not have saturated at low magnetic field in the case of i-SOC, as shown in the right panel.

At high magnetic fields, when  $E_Z > E_{VS}$ , our theory also captures the main features of  $1/T_1$ . It has a weaker dependence than  $B_0^5$  as a result of two main contributions to spin relaxation. One is due to the SVM and phonon noise that has a linear  $B_0$  dependence. The other is due to phonon noise via the intra-valley SOM, which has a  $B_0^5$  dependence at first but is suppressed at higher  $B_0$  due to the phonon bottleneck effect. The suppression of spin relaxation at higher  $B_0$  is indeed visible from the experimental data.  $1/T_1$  has a weaker  $B_0$ -dependence for the s-SOC compared to the case of the i-SOC, is again

from the different  $\mathcal{T}$ -symmetries of the two SOC mechanisms. Finally, near the SVH,  $1/T_1$  rises in a sharp peak, consistent with the experimental data.

Having obtained satisfactory consistency with experimental observations in spin relaxation, we turn to explore consequences of the  $\mathcal{T}$ -symmetry and the SVM on EDSR, spin-photon coupling, and spin pure dephasing.

*Enhanced EDSR and spin-photon coupling*— EDSR via SOM has been widely used in experiments for fast spin manipulation [12, 13, 15, 17, 39–43]. When an oscillating electric field of magnitude  $\vec{E}_0$  is applied, the electron spin experiences an effective oscillating magnetic field via the s-SOC induced SVM, which results in EDSR as well. The Rabi frequency  $\Omega_R$  of the EDSR is

$$\Omega_R(E_0) = eE_0 |\vec{r}^{v_0 v_1}| \eta_{SV} / \hbar. \quad (4)$$

where  $\eta_{SV}$  is given by Eq. (2). The Rabi frequency is thus enhanced via the constructive interference between the SVM paths as compared with i-SOC induced EDSR.

EDSR underlies recent efforts to reach the strong coupling limit between an electron spin and a cavity photon mode, where EDSR is driven by the vacuum electric field inside a superconducting resonator [14, 18, 19, 23, 44]. If the strong coupling limit can be achieved, the resulting circuit QED system can be used for quantum manipulation, communication, and measurement, which are crucial ingredients for a scalable quantum information processor. Here the vacuum Rabi splitting  $g_s = \Omega_R(E_{zpf})$  characterizes the spin-photon coupling strength, where  $E_{zpf} = V_{zpf}/l_0 = \omega_0 \sqrt{\hbar Z_0}/l_0$ ,  $V_{zpf}$  is the voltage amplitude due to the zero-point fluctuation (ZPF) in the resonator,  $\omega_0$  and  $Z_0$  the frequency and the characteristic impedance of the resonator, and  $l_0$  the length for the voltage drop [14, 44].

Fig. 3 top panels show the Rabi frequency  $\Omega_R$  and vacuum Rabi frequency  $g_s$  as a function of the magnetic field  $B_0$  due to the s-SOC (left panel) or the i-SOC (right panel). At low magnetic field when  $E_Z \ll E_{VS}$ , the Rabi frequency  $\Omega_R$  via the s-SOC induced SVM stays constant, while the vacuum Rabi frequency  $g_s$  grows linearly with  $B_0$  (photon energy grows as well). At  $B_0 = 0.1$  T,  $\Omega_R \sim 10^8$  s $^{-1}$  while  $g_s \sim 10^6$  s $^{-1}$ . In comparison, for the i-SOC,  $\Omega_R$  and  $g_s$  shows linear  $B_0$  and  $B_0^2$  dependence, respectively, and at 0.1 T,  $\Omega_R \sim 10^5$  s $^{-1}$  and  $g_s = 10^3$  s $^{-1}$ . As  $B_0$  increases,  $\Omega_R$  and  $g_s$  via the s- or i-SOC rise by orders of magnitude near the SVH. As the magnetic field  $B_0$  further increases past the hotspot,  $\Omega_R$  and  $g_s$  due to the SVM is reduced due to the reduced mixing, while the intra-valley SOM gradually becomes the dominant mechanism for EDSR or spin-photon coupling.

With SVM, pure dephasing for the spin qubit arises at the second order of s-SOC. The effective magnetic noise contributing to spin dephasing due to the SVM is (see Supplemental material)

$$n_{eff} = eV_{1/f}(r_{dip}/l_0) \sin \frac{\gamma + \gamma'}{2} \sin \frac{\gamma - \gamma'}{2}, \quad (5)$$

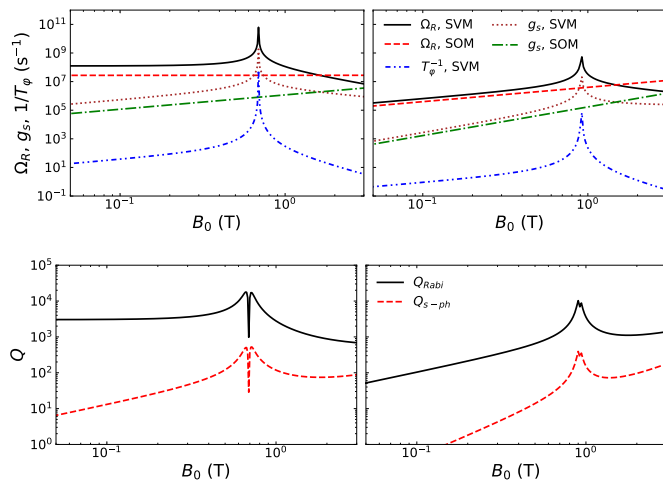


FIG. 3. Rabi frequency  $\Omega_R$ , Vacuum Rabi frequency  $g_s$ , pure dephasing  $1/T_\varphi$  (upper panels) and quality factors (lower panels) of Rabi driving and spin-photon coupling as a function of the magnetic field  $B_0$  for a spin in a silicon QD with the s-SOC (left panel) or the i-SOC (right panel). Both  $\Omega_R$  and  $g_s$  are increased near the SVH.

where  $V_{1/f}$  is the voltage fluctuation from the  $1/f$  charge noise, and  $r_{dip} = r^{v_0 v_0} - r^{v_1 v_1}$  is the dipole moment of the valley states. From the effective noise, the spin pure dephasing  $1/T_\varphi$  due to the SVM and the  $1/f$  charge noise can be evaluated [45, 46].

Fig. 3 top panels also show the spin pure dephasing rate  $1/T_\varphi$  as a function of the magnetic field  $B_0$  due to the  $1/f$  charge noise via the s- or i-SOC induced SVM. For both forms of SOC,  $1/T_\varphi$  has similar dependence on the magnetic field  $B_0$  and narrowly peaks at the SVH. However, given that the spin pure dephasing from other mechanisms is at least  $10^4$  s $^{-1}$  [8, 17, 47],  $1/T_\varphi$  due to the SVM is only relevant near the hotspot. Therefore, slightly away from the hotspot, before  $1/T_\varphi$  due to the SVM starts to dominate spin dephasing, the vacuum Rabi frequency (and also the Rabi frequency of EDSR) could be enhanced by orders of magnitude by tuning the valley splitting  $E_{VS}$  or the magnetic field  $B_0$  so that system is close to the point of SVH, while spin dephasing remains roughly constant.

*Quantum gate operation near the SVH*— The asynchronous rise of EDSR Rabi frequency  $\Omega_R$  and total spin dephasing near the SVH hints that one could possibly perform fast and high-fidelity quantum gates in this regime. Considering that spin relaxation is generally slower than pure dephasing, even at the hotspot, the total decoherence rate can be estimated as  $1/T_2^* = 1/T_\varphi + 1/T_{\varphi,other}$ , where  $1/T_{\varphi,other}$  originates from other sources such as nuclear spins or charge noise via longitudinal gradient [17]. Recent experiments show that  $1/T_{\varphi,other} \sim 5 \times 10^4$  s $^{-1}$  with micromagnets [17] (or  $1/T_{\varphi,other} \sim 1 \times 10^4$  s $^{-1}$  without micromagnets [8, 47]),

typical for a spin qubit in an isotopically purified Si QD. With  $\Omega_R$  characterizing how fast a single-qubit gate can be, the single-qubit quality factor can then be defined as  $Q_{Rabi} = \Omega_R T_2^*/(2\pi)$ , which is a measure of how well one can control such a qubit.

Fig. 3 (lower left panel) shows that the quality factor  $Q_{Rabi}$  with the s-SOC increases by an order of magnitude from  $10^3$  to  $10^4$  as the system approaches the SVH, before dephasing due to the SVM starts to dominate. If the spin qubit is coupled to a superconducting resonator, with the resonator decay rate  $\kappa$  and the bare spin decoherence rate  $1/T_{\varphi,other}$  both  $\sim 5 \times 10^4$  s $^{-1}$ , the strong coupling limit of  $g_s > \kappa, 1/T_2^*$  can be achieved when the system approaches the SVH. Indeed, Fig. 3 (lower right panel) shows that the quality factor  $Q_{s-ph} = g_s T_2^*/(2\pi)$  of spin-photon coupling can reach above  $10^2$ . In short, by using the SVM near the hotspot, fast high-fidelity quantum gates are within reach for Si quantum computing.

The trend for the qubit quality factor to reach its peaks near the SVH holds for i-SOC as well. Fig. 3 (lower right panel) shows that the quality factors  $Q_{Rabi}$  and  $Q_{s-ph}$  without micromagnets can also be improved by orders of magnitudes near the SVH, which can be useful for high fidelity quantum gates without micromagnets, although the operation speed is slower than the case of the s-SOC.

Note that valley splitting in Si can be tuned electrically using top gates [26, 29]. Thus, one can electrically tune the valley splitting to turn on the SVM for spin manipulation and spin-spin coupling, and turn off the SVM for the idling qubits. Furthermore, with the SVM boosted EDSR in a single QD instead of a double QD [14, 18, 21, 23, 48], a spin-qubit-based architecture could be simplified without sacrificing manipulation speed and tunability.

*Conclusion*— In conclusion, we studied the theory of the spin relaxation and manipulation via the s-SOC from a micro-magnet. We find that qualitatively different behaviors of spin relaxation mediated by the s-SOC arise from the breaking  $\mathcal{T}$ -symmetry of the s-SOC. Our theory explains the experimentally observed field dependence of spin relaxation, at both low and high magnetic field regimes, and not captured by previous theories. Furthermore, we show that an enhancement of EDSR mediated by the s-SOC and the resulting SVM is a consequence of the constructive interference and the strong mixing at the hotspot. Combining the our results on Rabi frequency and spin dephasing, we find that the parameter regime near (but not at) the SVH may provide an optimal point for fast and high-fidelity quantum gates for semiconducting quantum computing.

*Acknowledgment*— The authors thank J. R. Petta and F. Borjans for helpful discussions. P.H. acknowledges supports by the National Natural Science Foundation of China (No. 11904157), the Science, Technology and Innovation Commission of Shenzhen Municipality (No. ZDSYS20170303165926217, No.

JCYJ20170412152620376) and Guangdong Innovative and Entrepreneurial Research Team Program (Grant No. 2016ZT06D348); X.H. acknowledges support by US ARO via grant W911NF1710257.

---

\* huangph@sustech.edu.cn

- [1] D. Loss and D. P. DiVincenzo, Phys. Rev. A **57**, 120 (1998).
- [2] J. R. Petta, A. C. Johnson, J. M. Taylor, E. A. Laird, A. Yacoby, M. D. Lukin, C. M. Marcus, M. P. Hanson, and A. C. Gossard, Science **309**, 2180 (2005).
- [3] R. Hanson, L. P. Kouwenhoven, J. R. Petta, S. Tarucha, and L. M. K. Vandersypen, Rev. Mod. Phys. **79**, 1217 (2007).
- [4] J. J. L. Morton, D. R. McCamey, M. A. Eriksson, and S. A. Lyon, Nature **479**, 345 (2011).
- [5] F. A. Zwanenburg, A. S. Dzurak, A. Morello, M. Y. Simmons, L. C. L. Hollenberg, G. Klimeck, S. Rogge, S. N. Coppersmith, and M. A. Eriksson, Rev. Mod. Phys. **85**, 961 (2013).
- [6] A. M. Tyryshkin, S. Tojo, J. J. L. Morton, H. Riemann, N. V. Abrosimov, P. Becker, H.-J. Pohl, T. Schenkel, M. L. W. Thewalt, K. M. Itoh, and S. A. Lyon, Nat Mater **11**, 143 (2012).
- [7] J. T. Muhonen, J. P. Dehollain, A. Laucht, F. E. Hudson, R. Kalra, T. Sekiguchi, K. M. Itoh, D. N. Jamieson, J. C. McCallum, A. S. Dzurak, and A. Morello, Nat. Nanotechnol. **9**, 986 (2014).
- [8] M. Veldhorst, C. H. Yang, J. C. C. Hwang, W. Huang, J. P. Dehollain, J. T. Muhonen, S. Simmons, A. Laucht, F. E. Hudson, K. M. Itoh, A. Morello, and A. S. Dzurak, Nature **526**, 410 (2015).
- [9] D. M. Zajac, A. J. Sigillito, M. Russ, F. Borjans, J. M. Taylor, G. Burkard, and J. R. Petta, Science **359**, 439 (2018).
- [10] T. F. Watson, S. G. J. Philips, E. Kawakami, D. R. Ward, P. Scarlino, M. Veldhorst, D. E. Savage, M. G. Lagally, M. Friesen, S. N. Coppersmith, M. A. Eriksson, and L. M. K. Vandersypen, Nature (2018), 10.1038/nature25766.
- [11] W. Huang, C. H. Yang, K. W. Chan, T. Tanttu, B. Hensen, R. C. C. Leon, M. A. Fogarty, J. C. C. Hwang, F. E. Hudson, K. M. Itoh, A. Morello, A. Laucht, and A. S. Dzurak, Nature **569**, 532 (2019).
- [12] Y. Tokura, W. G. van der Wiel, T. Obata, and S. Tarucha, Phys. Rev. Lett. **96**, 047202 (2006).
- [13] M. Pioro-Ladriere, T. Obata, Y. Tokura, Y.-S. Shin, T. Kubo, K. Yoshida, T. Taniyama, and S. Tarucha, Nature Physics **4**, 776 (2008).
- [14] X. Hu, Y.-x. Liu, and F. Nori, Phys. Rev. B **86**, 035314 (2012).
- [15] E. Kawakami, P. Scarlino, D. R. Ward, F. R. Braakman, D. E. Savage, M. G. Lagally, M. Friesen, S. N. Coppersmith, M. A. Eriksson, and L. M. K. Vandersypen, Nat. Nanotechnol. **9**, 666 (2014).
- [16] M. J. Rancic and G. Burkard, Phys. Rev. B **93**, 205433 (2016).
- [17] J. Yoneda, K. Takeda, T. Otsuka, T. Nakajima, M. R. Delbecq, G. Allison, T. Honda, T. Kodera, S. Oda, Y. Hoshi, N. Usami, K. M. Itoh, and S. Tarucha, Nat. Nanotechnol. **13**, 102 (2018).
- [18] X. Mi, M. Benito, S. Putz, D. M. Zajac, J. M. Taylor, G. Burkard, and J. R. Petta, Nature **555**, 599 (2018).
- [19] N. Samkharadze, G. Zheng, N. Kalhor, D. Brousse, A. Sammak, U. C. Mendes, A. Blais, G. Scappucci, and L. M. K. Vandersypen, Science **359**, 1123 (2018).
- [20] A. J. Landig, J. V. Koski, P. Scarlino, U. C. Mendes, A. Blais, C. Reichl, W. Wegscheider, A. Wallraff, K. Ensslin, and T. Ihn, Nature **560**, 179 (2018).
- [21] M. Benito, X. Croot, C. Adelsberger, S. Putz, X. Mi, J. R. Petta, and G. Burkard, Phys. Rev. B **100**, 125430 (2019).
- [22] F. Borjans, D. M. Zajac, T. M. Hazard, and J. R. Petta, Phys. Rev. Appl. **11**, 044063 (2019).
- [23] F. Borjans, X. G. Croot, X. Mi, M. J. Gullans, and J. R. Petta, Nature **577**, 195 (2020).
- [24] A. Hollmann, T. Struck, V. Langrock, A. Schmidbauer, F. Schauer, T. Leonhardt, K. Sawano, H. Riemann, N. V. Abrosimov, D. Bougeard, and L. R. Schreiber, Phys. Rev. Appl. **13**, 034068 (2020).
- [25] T. Struck, A. Hollmann, F. Schauer, O. Fedorets, A. Schmidbauer, K. Sawano, H. Riemann, N. V. Abrosimov, L. Cywinski, D. Bougeard, and L. R. Schreiber, NPJ Quantum Inf. **6**, 1 (2020).
- [26] X. Zhang, R.-Z. Hu, H.-O. Li, F.-M. Jing, Y. Zhou, R.-L. Ma, M. Ni, G. Luo, G. Cao, G.-L. Wang, X. Hu, H.-W. Jiang, G.-C. Guo, and G.-P. Guo, Phys. Rev. Lett. **124**, 257701 (2020).
- [27] P. Huang and X. Hu, arXiv:2008.04671 (2020).
- [28] P. Y. Yu and M. Cardona, *Fundamentals of Semiconductors* (Springer-Verlag, Berlin, Germany, 2010).
- [29] C. H. Yang, A. Rossi, R. Ruskov, N. S. Lai, F. A. Mohiyaddin, S. Lee, C. Tahan, G. Klimeck, A. Morello, and A. S. Dzurak, Nat. Commun. **4**, 2069 (2013).
- [30] P. Huang and X. Hu, Phys. Rev. B **90**, 235315 (2014).
- [31] W. Huang, M. Veldhorst, N. M. Zimmerman, A. S. Dzurak, and D. Culcer, Phys. Rev. B **95**, 075403 (2017).
- [32] P. Huang and G. W. Bryant, Phys. Rev. B **98**, 195307 (2018).
- [33] A. Corna, L. Bourdet, R. Maurand, A. Crippa, D. Kotekar-Patil, H. Bohuslavskiy, R. Laviéville, L. Hutin, S. Barraud, X. Jehl, M. Vinet, S. De Franceschi, Y.-M. Niquet, and M. Sanquer, NPJ Quantum Inf. **4**, 1 (2018).
- [34] C. Tahan and R. Joynt, Phys. Rev. B **89**, 075302 (2014).
- [35] J. K. Gamble, M. A. Eriksson, S. N. Coppersmith, and M. Friesen, Phys. Rev. B **88**, 035310 (2013).
- [36] V. N. Golovach, A. Khaetskii, and D. Loss, Phys. Rev. Lett. **93**, 016601 (2004).
- [37] T. Meunier, I. T. Vink, L. H. Willems van Beveren, K.-J. Tielrooij, R. Hanson, F. H. L. Koppens, H. P. Tranitz, W. Wegscheider, L. P. Kouwenhoven, and L. M. K. Vandersypen, Phys. Rev. Lett. **98**, 126601 (2007).
- [38] P. Huang and X. Hu, Phys. Rev. B **89**, 195302 (2014).
- [39] V. N. Golovach, M. Borhani, and D. Loss, Phys. Rev. B **74**, 165319 (2006).
- [40] M. Borhani and X. Hu, Phys. Rev. B **85**, 125132 (2012).
- [41] K. C. Nowack, F. H. L. Koppens, Y. V. Nazarov, and L. M. K. Vandersypen, Science **318**, 1430 (2007).
- [42] S. Nadj-Perge, S. M. Frolov, E. P. a. M. Bakkers, and L. P. Kouwenhoven, Nature **468**, 1084 (2010).
- [43] M. D. Schroer, K. D. Petersson, M. Jung, and J. R. Petta, Phys. Rev. Lett. **107**, 176811 (2011).
- [44] A. Blais, R.-S. Huang, A. Wallraff, S. M. Girvin, and

- R. J. Schoelkopf, Phys. Rev. A **69**, 062320 (2004).
- [45] X. Hu and S. Das Sarma, Phys. Rev. Lett. **96**, 100501 (2006).
- [46] P. Huang, N. M. Zimmerman, and G. W. Bryant, NPJ Quantum Inf. **4**, 62 (2018).
- [47] M. Veldhorst, J. C. C. Hwang, C. H. Yang, A. W. Leenstra, B. d. Ronde, J. P. Dehollain, J. T. Muhonen, F. E. Hudson, K. M. Itoh, A. Morello, and A. S. Dzurak, Nat. Nanotechnol. **9**, 981 (2014).
- [48] X. Croot, X. Mi, S. Putz, M. Benito, F. Borjans, G. Burkard, and J. R. Petta, Phys. Rev. Research **2**, 012006 (2020), publisher: American Physical Society.